AN INVESTIGATION INTO THE INFLUENCES OF REFRIGERANTS' THERMAL-PHYSICAL PROPERTIES ON TEMPERATURE SEPARATION EFFECT OF A VORTEX TUBE

by

Zheng WANG[a*], Kwok On SUEN[b], and Zidong ZHAO[a]

[a] School of Civil Engineering and Architecture, Zhejiang Sci-Tech University, Hangzhou, China
[b] Department of Mechanical Engineering, University College London, London, United Kingdom

Original scientific paper
https://doi.org/10.2298/TSCI220926212W

The temperature separation effects of vortex tubes have been widely studied in open systems, using mainly air or N_2 as the working fluid. When a vortex tube is employed in a closed thermal system, more fluid choices, such as refrigerants, could be considered. Different to air, refrigerants have quite varied thermal-physical properties, and research of the thermal-physical properties' influence on the temperature separation effect is rather limited. Based on CFD simulated temperature separation effect of eight refrigerants (R152a, R290, R134a, R600a, R143a, R245fa, R227ea, and R218), this study attempts to gain a better insight into how their properties could be related to compare their temperature separation performance. The analysis shows for small mass-flow ratios at the cold end, the cooling effect can be assessed by the relative values of their isentropic expansion exponent. The results also suggest that a large thermal diffusivity and kinematic viscosity, and a small vapour density and Joule-Thomson coefficient would lead to better heating effects.

Key words: *vortex tube, temperature separation effect, refrigerants, CFD, thermal-physical properties*

Introduction

The vortex tube is a temperature separation device, and can be applied to generate a warmer and/or a colder fluid [1]. The performance of a vortex tube is usually defined in terms of its cooling effect, ΔT_c, and heating effect, ΔT_h, which are, respectively the decrease and increase in temperature at the cold and hot ends, with respect to the inlet temperature. Different working fluids are expected to generate dissimilar temperature separation effects even under the same operating conditions as they have different thermal-physical properties. Han *et al*. [2] experimented on N_2, CO_2, and some HFC (R32, R161, and R134a). They concluded that a large specific heat ratio (c_p/c_v) and a small thermal conductivity, λ, would lead to a large cooling effect, and a large kinetic viscosity, ν, would give rise to a large heating effect. In the test, the hot end throttle position was fixed at all conditions, resulting in the temperature separation effect being compared at different μ_c (the ratio of the colder fluid mass-flow rate and the vortex tube inlet mass-flow rate). But the μ_c is however generally regarded as an important factor in affecting temperature separation effect. Kargaran *et al*. [3] investigated the entropy generation for natural gas (CH_4, CO_2, N_2, C_2H_6, C_3H_8, C_4H_{10}, C_5H_{12}, and C_{6+}) and air. Their results indicated that the

* Corresponding author, e-mail: zheng.wang@zstu.edu.cn

lowest entropy can be obtained at the longest tube for natural gas while the middle tube for air. Aydin and Baki [4] experimentally compared the cooing effect of O_2, N_2, and air. They observed that, at a given μ_c, N_2 has the largest cooling effect and stated that was due to N_2 having the smallest molecular weight. One would therefore, expect O_2 to produce a smaller cooling effect than air as it is heavier than air, but no such result was noted.

Khazaei *et al*. [5] and Thakare and Parekh [6] numerically investigated the properties' influence on the vortex tube behaviour. In their models, the cold end was closed, *i.e*., the fluid only exited the hot end. Essentially, they were examining the expansion of a rotating flow and the associated temperature drop of various chosen fluids. Khazaei *et al*. [5] observed that He (among CO_2, air, NH_3, N_2, O_2, and water vapour) has the largest temperature drop, and they believed this is due to its largest specific heat ratio and smallest molecular weight. Thakare and Parekh's [6] study indicates that, for the individual gas (He, H_2, N_2, and O_2), thermal diffusivity α is the dominated affecting parameter on the temperature drop. For the compound gas (CH_4, vapour water, air and CO_2), the variation behaviour of the temperature drop is quite analogous to that of the λ.

The CFD is a research tool employed to study and predict the temperature separation effect of vortex tube under various conditions [7, 8]. Frohlingsdorf and Unger [9] developed a 2-D vortex tube geometry with *k-ε* turbulence model. They analysed the flow process through the vortex tube, and noticed a circulating secondary flow which receives the energy from the cold air and transfers outward to the hot air. Karimi-Esfahani *et al*. [10] used their 2-D vortex tube model to optimize the vortex tube dimensions and operating condition for producing the largest ΔT_c. Aljuwayhel *et al*. [11] compared the Standard *k-ε* and the RNG *k-ε* turbulence models by employing their 2-D geometry, and noted that predicted results by the Standard *k-ε* model matched well with the experimental data. Nezhad and Shamsoddini [12] established a 3-D model, using the RNG *k-ε* model, to investigate the energy separation mechanism and compared the results of their 3-D model with their previous established 2-D. Dutta *et al*. [13] defined a 3-D vortex tube geometry, and compared four turbulence models: standard *k-ε*, RNG *k-ε*, standard *k-ω* and SST *k-ω*, the results showed that the standard k-ε turbulence model produced a better agreement of T_c and T_h with the experiments.

In general, it can be noted that the comparative analysis of fluid properties' influence on temperature separation effect is often based on a relatively small group of fluid choices such as air, O_2, and N_2. As more research on the use of vortex tube in the closed systems are being conducted [14, 15], this opens up the possibility of considering more fluid options, such as refrigerants. In fact, refrigerants normally have different thermal-physical behaviours than air (or O_2, N_2), such as refrigerants always have a higher critical point (*e.g*. R32 has 78.11 °C [16], air has –140.31 °C). This may bring a non-ideal gas behaviour in vortex tube than air [17]. So, the observations of properties' influence mainly based on air from previous research may be not suitable to assess the temperature separation effect of different refrigerants. Then, this research attempts to provide a detailed analysis of refrigerants' thermal-physical properties' influences on temperature separation effect. The CFD code ANSYS FLUENT is employed to carry the numerical analysis. Eight real-gas model refrigerants' (R152a, R290, R134a, R600a, R143a, R245fa, R227ea, and R218) are chosen to gain a better insight into how their properties could be related to compare their temperature separation performance.

The CFD model

Geometry definition and mesh number selection

Using ANSYS FLUENTl, a 2-D vortex tube geometry based on the primary vortex tube dimensions of Aljuwayhel *et al*. [11] is set up, fig. 1. As adopted by [11], an axial annular inlet is chosen, that is expected to lead to a relatively quicker convergence in simulation compared to a radial annular slot. The annular inlet is actually the vortex tube chamber inlet. The chamber inlet total pressure and temperature are in fact equal to the vortex tube nozzle inlet ones which in terms have approximately the same values at the static pressure and temperature. The axial, tangential and radial components at the inlet can be specified to achieve the desired entry angle. As in [17], five turbulence models: *k*-*ε* standard, *k*-*ε* RNG, *k*-*ε* RNG (swirl), *k*-*ω* SST, and *k*-*ω* standard, are chosen for this study. The preliminary iteration using the first order upwind method [18] is employed to obtain quickly the initial approximated results, based on the defaulted under-relax factors. The convergent target for continuity is set at 0.0001, and at 0.00001 for the *x*-velocity, *y*-velocity, swirl and energy. The primary iteration employed the second order upwind method [18] to obtain the final results. Lower than the default values of under-relax factors are then used to achieve a smaller convergent target.

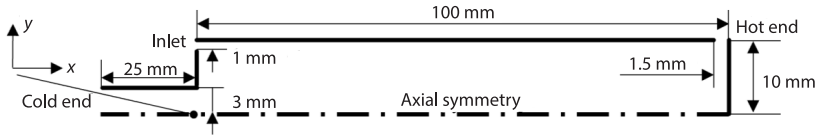

Figure 1. Vortex tube geometry and dimensions of the CFD model

Meshing element numbers varying from around 30000-160000 at an increment of approximately 20000 were trialled. Convergence is considered achieved, fig. 2, when the element number is increased to 90000, and the incremental changes, Δ, of the ΔT_c and ΔT_h are tiny (drop to below 0.1 °C). It is considered not justified to further increase the elements number to 110000 as it only marginally improved the accuracy but almost doubled pc run time. Then, the meshing element number around 90000 is chosen in this study.

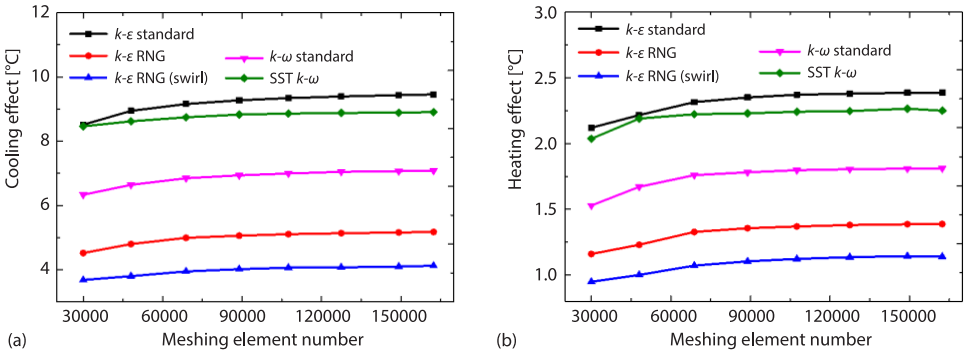

Figure 2. Cooling effect (a) and heating effect (b) change with various meshing element numbers for different turbulence models (μ_c = 0.2, $\dot{m}_{in}$ = 3.9 g/s, p_c = 1 bar, air)

Quantitative and qualitative validations

The boundary conditions are set to match with the experimental set-up of [11]: the inlet air $\dot{m}_{in}$ are 3.9 and 4.0 g/s, respectively for μ_c = 0.2 and 0.1, and the T_{in} is set at 22 °C, the p_c is fixed at 1 bar (absolute), the hot end pressure is varied to control the μ_c. The CFD results

by chosen turbulence models and the experimental results of [11] are compared in tab. 1. It indicates that the *k-ε* standard model shows quite a good match with the experimental results. Hence the standard *k-ε* model is chosen.

Table 1. Comparison of simulated results and experiment results (μ_c = 0.2, $\dot{m}_{in}$ = 3.9 g/s air)

Models	ΔT_c [°C]	ΔT_h [°C]
Experiment [11]	9.4 ±0.2	2.0 ±0.2
k-ε standard	9.3	2.3
k-ε RNG	5.1	1.4
k-ε RNG (swirl)	4.1	1.1
k-ω SST	8.8	2.3
k-ω standard	4.1	1.1

Table 2. Comparison of simulated results and experiment results (μ_c = 0.1, $\dot{m}_{in}$ = 4.0 g/s air)

Models	ΔT_c [°C]	ΔT_h [°C]
Experiment [11]	11 ±0.2	1.2 ±0.2
k-ε standard	10.9	1.3
k-ε RNG	7.2	0.9
k-ε RNG (swirl)	5.9	0.8
k-ω SST	10.7	1.3
k-ω standard	8.6	1.1

The *k-ε* standard turbulence model, in which the turbulence kinetic energy k and the rate of dissipation ε, can be obtained from the following transport equations [19]:

$$\frac{\partial(\rho k)}{\partial t}+\frac{\partial(\rho k u_i)}{\partial x_i}=\frac{\partial}{\partial x_j}\left[\left(\mu+\frac{\mu_t}{\sigma_k}\right)\frac{\partial k}{\partial x_j}\right]+G_k+G_b-\rho\varepsilon-Y_M+S_k \tag{1}$$

$$\frac{\partial(\rho\varepsilon)}{\partial t}+\frac{\partial(\rho\varepsilon u_i)}{\partial x_i}=\frac{\partial}{\partial x_j}\left[\left(\mu+\frac{\mu_t}{\sigma_e}\right)\frac{\partial\varepsilon}{\partial x_j}\right]+C_{1\varepsilon}\frac{\varepsilon}{k}(G_k+C_{3\varepsilon}G_b)-C_{2\varepsilon}\rho\frac{\varepsilon^2}{k}+S_\varepsilon \tag{2}$$

where G_k is the generation of turbulence kinetic energy from the mean velocity gradients, G_b – the generation of turbulence kinetic energy from buoyancy, Y_M – the contribution of the fluctuating dilatation in compressible turbulence to the overall dissipation rate, $C_{1\varepsilon}$, $C_{2\varepsilon}$, $C_{3\varepsilon}$ are the constants, σ_k and σ_ε – the turbulent Prandtl numbers for k and ε, S_k and S_ε – the user-defined source terms, and μ_t – the turbulent viscosity, which can be calculated by k and ε:

$$\mu_t=\rho C_\mu\frac{k^2}{\varepsilon} \tag{3}$$

where C_μ = 0.09, $C_{1\varepsilon}$ = 1.44, $C_{2\varepsilon}$ = 1.92, σ_k = 1.0, and σ_ε = 1.3

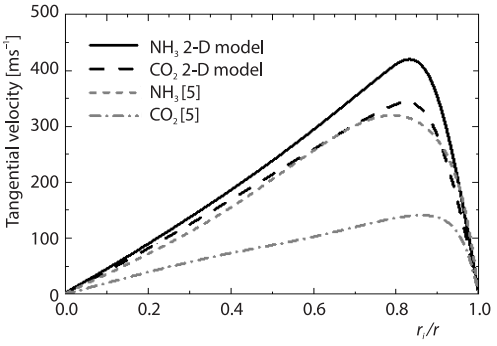

Figure 3. Predicted tangential velocities of CO_2 and NH_3 at x/Φ_{cham} = 2 and [5] results

In addition, the current vortex tube model is re-set-up to have the same *wall* boundary condition as in Khazaei *et al*. [5], also running at the same inlet mass-flow of 218.4 g/s and inlet total temperature of 24 °C for two fluids, NH_3 (R717) and CO_2 (R744). Predicted tangential velocities at the cross-section 40 mm away from the vortex tube inlet are depicted in fig. 3, and the velocities at the same distance, x, to diameter, Φ_{cham}, ratio, x/Φ_{cham}, from [5] are also plotted for comparison.

In both studies, the NH_3 is found to have higher tangential velocities than CO_2. Qualitatively the velocity profiles match very well, though the current model predicts much higher velocities, and smaller velocity differences between the two fluids, probably due to, respec-

tively the use of a much smaller vortex tube inlet area than in [5], and a smaller density difference between CO_2 and NH_3 under the current specified vortex tube inlet conditions. The results from the validations suggest that the current model set-up is capable of predicting reliably the temperature separation effect and flow characteristics of the vortex tube for the chosen refrigerants.

Results and discussion

The temperature separation effect of eight commercially available refrigerants R152a, R290, R134a, R600a, R143a, R245fa, R227ea, and R218 are compared and analysed. Two vortex tube inlet conditions (1.2 bar and 30 °C, and 1.5 bar and 35° C) are used, both to ensure all chosen refrigerants entering the vortex tube in vapour state [20]. The cold end is fixed at 1 bar absolute pressure and the hot end pressure is varied to control the μ_c (0.1-0.9). The cooling effect of the refrigerants are shown in fig. 4 for the vortex tube inlet at 1.2 bar and 30 °C.

For a given refrigerant, in general a higher μc would give rise to a lower cooling effect. This is due to the fact that smaller vortex tube chamber inlet velocities are produced at higher μ_c, fig. 5. As stated in Eiamsa-ard [21], a higher tangential velocity has a larger momentum transfer from the inner to the outer layers of the rotating flow in the vortex tube, thus generating a larger temperature separation effect. With a small μ_c (< 0.5), R152a has the largest cooling effect, followed by the fluid R290, R143a, R134a, R600a, and R245fa, while R227ea and R218 generate the smallest cooling effect. At higher μ_c (> 0.5), their relative rankings (though alter slightly) become practically insignificant, as all refrigerants have rather small cooling effect (less than 1 °C), and the vortex tube would be mainly used for heating [22, 23].

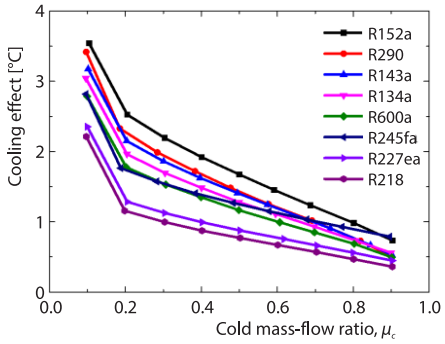

Figure 4. Cooling effect for eight refrigerants at P_{in} = 1.2 bar, T_{in} = 30 °C

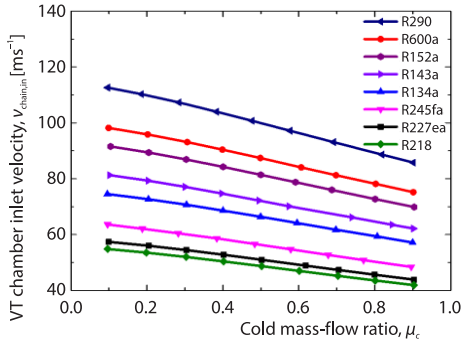

Figure 5. Vortex tube chamber inlet velocity for eight refrigerants at p_{in} = 1.2 bar, T_{in} = 30 °C

Figure 6 displays the tangential velocities and the corresponding tangential shear stresses τ_{wy} (= $v_{gradient} \times \mu$) in the radial direction for R152a, R600a, and R218, at two cross-sections CS1 and CS2 (respectively at x_1 = 2 mm and x_2 = 90 mm, away from the chamber inlet in positive axial direction) for μ_c = 0.2. As expected, at any locations, higher stresses are usually associated steep velocity gradients as seen in fig. 6. Though R600a has a slightly stronger rotation (*i.e.*, larger tangential velocities) than R152a, the latter has largest shear stresses which favour the generation of stronger temperature separation, as reflected in fig. 4. Among these three, R218 has the smallest temperature separation effect, as it has both the smallest shear stresses and tangential velocities. When the fluid rotates from CS1 to CS2, both the tangential velocity and shear stress decrease, indicating that the rotation becomes weaker due to the friction. For all fluids, at a given cross-section, the tangential velocity and shear stress at central area are

much smaller than that at the peripheral area, suggesting the temperature separation effect from rotation may mainly happen at the outer of the tube.

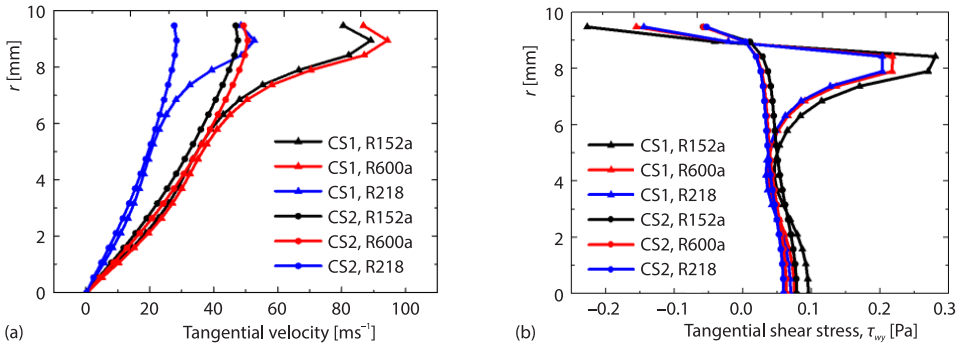

Figure 6. Tangential velocities (a) and tangential shear stress τ_{wy} (b) for R152a, R600a and R218 at two cross-sections (CS1: x_1 = 2 mm, CS2: x_2 = 90 mm), with μ_c = 0.2

The cooling effect of a vortex tube is expected to be smaller than the isentropic temperature drop and the isentropic expansion is the primary process for cooling effect inside the vortex tube [24]. Table 2 presents the calculated isentropic temperature drop (in descending order) and isentropic expansion exponent $\kappa = -v/p(\partial p/\partial v)_s$ [25], for these refrigerants all under the same vortex tube inlet and cold end conditions. They follow rather closely the ranking order of the refrigerants' cooling effect for small μ_c (< 0.5) (as presented in fig. 4). As the pressure drop between the inlet and cold end is kept constant, this observation suggests it may be possible to use the κ to rank their cooling performance, that can be determined using relatively simple thermodynamics calculations [25]. For a constant pressure ratio, in general a larger isentropic expansion exponent κ would lead to a smaller outlet temperature, hence a larger cooling effect.

Table 2. Ranking of cooling effect for chosen refrigerants and their isentropic temperature drop and isentropic expansion exponent κ (p_{in}= 1.2 bar, T_{in}=30 °C, p_c= 1 bar)

Ranking, ΔT_c	Refrigerant	ΔT_s [°C]	κ
1	R152a	6.95	1.13
2	R290	6.32	1.11
3	R143a	5.97	1.11
4	R134a	5.54	1.09
5	R600a	4.92	1.07
6	R245fa	4.32	1.05
7	R227ea	3.55	1.04
8	R218	3.22	1.04

Figure 7 shows the heating effect at p_{in} = 1.2 bar and T_{in} = 30 °C. For a given refrigerant, the heating effect increases with increasing μ_c. Lower vortex tube inlet velocities, fig. 5, are encountered at high μ_c values and therefore, smaller heating effect (temperature rise) should be expected. However, on the other hand the associated smaller pressure drops between the vortex tube inlet and the hot end, $\Delta p_{in\text{-}h}$, fig. 8, would lead to smaller temperature drops for these

refrigerants, thus producing a net increase in the heating effect. It is useful to point out at this stage that though all the refrigerants have rather similar $\Delta p_{\text{in-h}}$, the temperature drop associated with this expansion process varies amount individual refrigerants, depending on their properties.

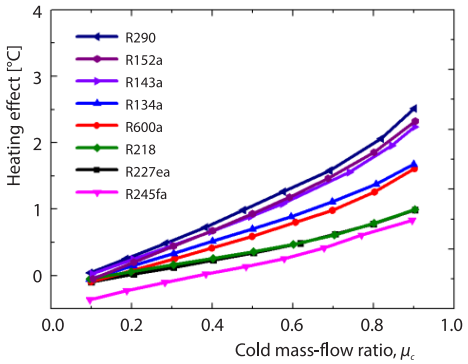

Figure 7. Heating effect for eight refrigerants at p_{in} = 1.2 bar, T_{in} = 30 °C

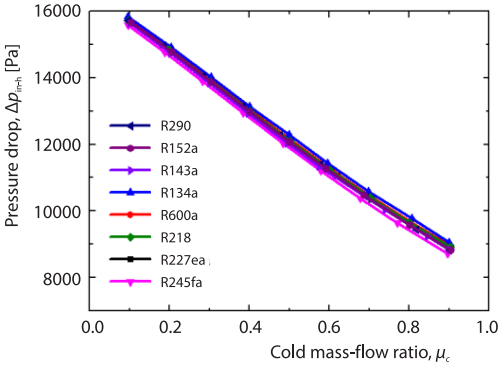

Figure 8. Pressure drop through the vortex tube inlet and hot end at p_{in} = 1.2 bar, T_{in} = 30 °C

For the heating effect, the simulations show that R290, R152a and R143a are better performers, followed by R134a and R600a; R218, R227ea and R245fa have the smallest heating effect. This study looks into if it is possible to rely upon certain refrigerant's thermal-physical properties to assess the relatively ranking of their heating effect. As the temperature separation effect involves heat transfer and frictional sheers between rotating fluid layers, and based on previous studies [2, 4-6], the thermal conductivity, λ, specific heat capacity c_p, dynamic viscosity μ and density ρ are initially appraised.

A *fictitious* fluid is created for which λ, c_p, μ, and M are independently and *artificially* defined in the FLUENT fluid property when setting up the CFD runs. For each of the CFD runs, only one of the parameters is varied while the other three are kept constant. Molecular weight, M, is used instead of the density ρ because the temperature separation effect could not be produced when the density, ρ, is set as a constant value. Tables 3-6 present the effect of λ, c_p, μ, and M on the temperature separation effect, at the following conditions: p_{in} = 3 bar, T_{in} = 295 K, p_{c} = 1 bar, and p_{h} = 2 bar.

Table 3. Effect of thermal conductivity λ

λ [mWm^{-1}K^{-1}]	ΔT_{c} [°C]	ΔT_{h} [°C]
100	14.95	14.32
200	14.96	14.34
300	14.98	14.35
400	15.00	14.37
500	15.01	14.38
600	15.03	14.39

Table 4. Effect of molecular weight M

M [kgkmol^{-1}]	ΔT_{c} [°C]	ΔT_{h} [°C]
40	11.26	10.47
70	6.60	6.30
100	4.73	4.46
130	3.69	3.45
160	3.03	2.81
190	2.57	2.38

Based on the results, it can be noted that a larger λ, or a smaller specific heat capacity c_p, or a smaller M would lead to a larger ΔT_{c} and ΔT_{h}, but the influence of λ appears to be rather marginal. In addition, and a smaller μ would lead to a larger ΔT_{c} and a smaller ΔT_{h}, though the influence of μ appears to be relatively minor.

Table 5. Effect of specific heat capacity c_p

c_p [kJkg^{-1}K^{-1}]	ΔT_c [°C]	ΔT_h [°C]
0.8	18.53	17.38
0.9	16.54	15.70
1.0	14.93	14.32
1.1	13.61	13.15
1.2	12.51	12.15
1.3	11.56	11.29

Table 6. Effect of viscosity μ

μ [uPa·s]	ΔT_c [°C]	ΔT_h [°C]
7	22.89	19.49
8	22.63	19.54
9	22.40	19.58
10	22.19	19.61
11	21.99	19.64
12	21.81	19.67

Table 7 displays the chosen physical-thermal properties of refrigerants at the specified vortex tube inlet conditions (30 °C and 1.2 bar). Relatively speaking the refrigerants having a larger ΔT_h do not always have a larger λ and μ, and smaller c_p and M, indicating that it is not always reliable to assess the relative temperature separation effect of refrigerants based on individual properties.

Table 7. Physical-thermal properties of chosen refrigerants at T_{in}=30 °C, p_{in}= 1.2 bar

Refrigerant (Ranking for ΔT_h)		λ [mW/m^{-1}K^{-1}]	c_p [kJkg^{-1}K^{-1}]	M [kgmol^{-1}]		μ [uPa·s]	
R290	(1)	18.87 (1)	1.71 (1)	44.10	(8)	8.28	(7)
R152	(2)	14.66 (4)	1.07 (3)	66.00	(6)	10.26	(6)
R143a	(3)	15.35 (3)	0.96 (4)	84.00	(5)	11.27	(4)
R134a	(4)	13.80 (5)	0.86 (6)	102.03	(4)	12.01	(2)
R600a	(5)	17.41 (2)	1.72 (2)	58.12	(7)	7.62	(8)
R218	(6)	12.93 (8)	0.81 (8)	188.02	(1)	12.70	(1)
R227ea	(7)	13.71 (6)	0.82 (7)	170.03	(2)	11.79	(3)
R245fa	(8)	13.27 (7)	0.93 (5)	134.05	(3)	10.62	(5)

However, when based on the thermal diffusivity, α (= $\lambda/\rho c_p$), the kinematic viscosity, ν (= μ/ρ), and the density, ρ, of the eight chosen refrigerants, as listed in the descending order of thermal diffusivity in tab. 8, it is noted that the kinematic viscosity follows the same order, and both α and ν are found to match fairly well with the ranking of their heating effect, especially among the top performers. This is somewhat expected as the thermal diffusivity [26] represents the rate of heat transferring into the medium during changes in temperature with time, and a larger α corresponds to a faster propagation of heat into the medium. The kinematic viscosity (also referred as momentum diffusivity [27]) expresses the propagation of the movement by friction.

The R290, having the highest values of both α and ν, and with the smallest density ρ, produces the highest heating effect. At the bottom half, R218, with the lowest values of α and ν, and the largest ρ, does not have the lowest heating effect. There is a *slight* mis-match between the ranking orders of α and ΔT_h, especially for refrigerants with weak heating effects. It is believed that the heating effect (temperature rise) created from the rotational process could be cancelled out by the temperature drop resulted from the adiabatic expansion through the vortex tube [17]. As the latter could be related to J-T effect, the author is to assess whether J-T coefficient [28, 29] could be used to help us to understand better the relative ranking of the heating effect.

Table 9 presents the J-T isenthalpic temperature drops based on the specified inlet (30 °C and 1.2 bar) and the corresponding hot end pressures at $\mu_c = 0.8$, and the J-T coefficient, μ_{JT}. The R245fa has the largest μ_{JT}, thus giving rise to the biggest isenthalpic temperature drop that cancels out a big part of the heating effect, resulting in placing it at the bottom of the heating effect ranking, as seen in fig. 7.

Table 8. Physical-thermal properties of chosen refrigerants at T_{in}=30 °C, p_{in}= 1.2 bar

Refrigerant (Ranking for ΔT_h)		α [cm^{2}s^{-1}]	ν [cm^{2}s^{-1}]	ρ [kgm^{-3}]
R290	(1)	0.051 (1)	0.038 (1)	2.17 (8)
R152a	(2)	0.042 (2)	0.031 (2)	3.27 (6)
R143a	(3)	0.039 (3)	0.027 (3)	4.14 (5)
R600a	(5)	0.035 (4)	0.026 (4)	2.89 (7)
R134a	(4)	0.032 (5)	0.024 (5)	5.04 (4)
R245fa	(8)	0.021 (6)	0.015 (6)	6.79 (3)
R227ea	(7)	0.020 (7)	0.014 (7)	8.47 (2)
R218	(6)	0.017 (8)	0.014 (8)	9.30 (1)

Table 9. The J-T isenthalpic temperature drops and J-T coefficient (T_{in} = 30 °C, p_{in} = 1.2 bar, μ_c = 0.8)

Refrigerant	J-T temperature drop [°C]	J-T coefficient μ_{JT} [°CMPa^{-1}]
R245fa	0.36	38.09
R152a	0.26	26.58
R600a	0.20	20.91
R134a	0.20	20.48
R143a	0.17	17.79
R227ea	0.17	17.25
R290	0.16	16.31
R218	0.12	12.07

Based on the aforementioned observations and discussions, it can be preliminarily concluded that isentropic expansion exponent, κ, thermal diffusivity, α, kinematic viscosity, ν, J-T coefficient, μ_{JT}, and density, ρ, (or molecular weight M) can be used to help assessing the relative temperature separation effect ranking of refrigerants. To achieve a better cooling effect, a fluid should have a large isentropic expansion exponent, and to achieve a better heating effect, a fluid should have a small density and J-T coefficient, and a large thermal diffusivity and kinematic viscosity.

To further examine the validity of the approach, two natural refrigerants CO_2 and NH_3 are chosen to have their temperature separation effect compared firstly based on their properties and the on the CFD results. Table 10 displays the associated properties for CO_2, NH_3, R290, and R152a. The NH_3 has the largest isentropic expansion exponent, κ, followed by CO_2, then R152a, and R290. Based on the previous discussion, this suggests that NH_3 could produce the largest cooling effect, then followed by CO_2, R152a, and R290. In addition, NH_3 has the largest

thermal diffusivity, α, kinematic viscosity, ν, and the smallest density, ρ, implying that it could also produce the highest heating effect. However, NH_3 has a quite large J-T coefficient, μ_{JT}, thus its J-T temperature drop could potentially cancel a large amount of the heating effect, that could send its heating ranking down the list. On the other hand, for CO_2, its α, ν, and ρ all rank lower than NH_3, but its μ_{JT} is much smaller than that of NH_3, and this could help to propel it to top of the heating effect ranking than, higher NH_3.

Table 10. Physical-thermal properties of chosen refrigerants at T_{in}=30 °C, p_{in}= 1.2 bar

Refrigerant	κ	α [cm^{2}s^{-1}]	ν [cm^{2}s^{-1}]	ρ [kgm^{-3}]	μ_{JT} [°CMPa^{-1}]
NH_3	1.30 (1)	0.140 (1)	0.123 (1)	0.83 (1)	26.45 (2)
CO_2	1.29 (2)	0.093 (2)	0.071 (2)	2.14 (2)	10.48 (4)
R290	1.11 (4)	0.051 (3)	0.038 (3)	2.17 (3)	16.31 (3)
R152a	1.13 (3)	0.042 (4)	0.031 (4)	3.27 (4)	26.58 (1)

Figure 9 shows the CFD simulated cooling and heating effect for refrigerants, showing that NH_3 produces the largest cooling effect, followed by CO_2, R152a and R290, and CO_2 produced the largest heating effect, followed by NH_3, R290, and R152a. This trend match very well with the prediction based on the properties ranking. When the analysis is repeated at a higher inlet temperature and pressure (T_{in} = 35 °C and p_{in} = 1.5 bar), exactly the same observations are noted.

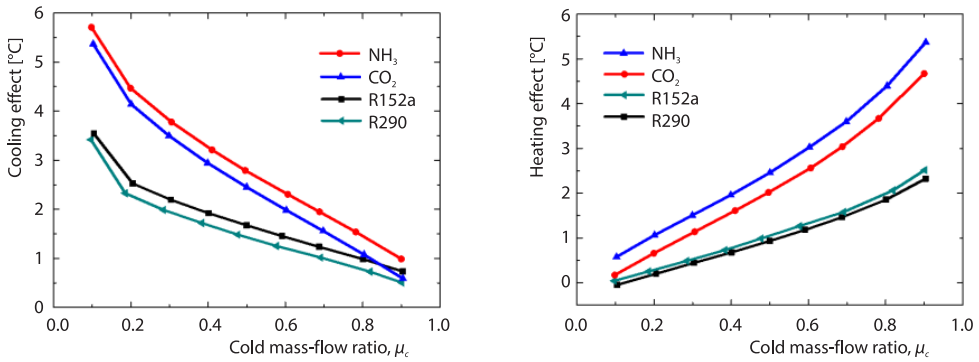

Figure 9. Temperature separation effect of NH_3, CO_2, R152a, and R290 at T_{in} = 30 °C, p_{in} = 1.2 bar

Conclusions

The influence of thermal-physical properties on the temperature separation effect is numerically investigated and compared. Relative influence of certain refrigerant properties on the temperature separation effect are discussed and the following conclusions can be drawn.

For all the chosen refrigerants, the vortex tube can provide relatively more cooling effect at a smaller cold mass-flow ratio μ_c (<0.5), while more heating effect at a larger μ_c value (>0.5). The tangential velocity and shear stress at the core are found to be much smaller than that at the peripheral area, suggesting the temperature separation effect mainly come from the outer region of the tube. The refrigerant having higher cooling effect has a larger shear stress, which generate larger friction in the rotation flow.

At all examined vortex tube inlet operating conditions, the relative ranking of the cooling effect can be assessed by the isentropic expansion exponent of the refrigerants. A single thermal-physical property could not be used individually to estimate the relative heating effect.

To achieve a large heating effect, the fluid should have a small density and J-T coefficient and a large thermal diffusivity and kinematic viscosity at the vortex tube inlet conditions. A small density and J-T coefficient, respectively contribute towards a stronger rotating at the vortex tube chamber and small temperature cancelling for the heating effect.

Nomenclature

c_p – specific heat capacity at constant pressure, [kJkg^{-1}K^{-1}]
c_v – secific heat capacity at constant volume, [kJkg^{-1}K^{-1}]
k – turbulence kinetic energy, [m^{2}s^{-2}]
M – molecular mass, [kgkmol^{-1}]
$\dot{m}$ – mass-flow rate, [gs^{-1}]
p – pressure, [bar]
r – radius, [mm]
T – temperature, [°C]
ΔT_c – T_{in}–T_c, cooling effect, [°C]
ΔT_h – T_h–T_{in}, heating effect, [°C]
ΔT_s – isentropic temperature drop, [°C]
v – velocity, [ms^{-1}]

Greek letters

α – thermal diffusivity [cm^{2}s^{-1}]
ε – dissipation rate, [m^{2}s^{-3}]
κ – isentropic expansion exponent
λ – thermal conductivity [Wm^{-1}K^{-1}]
μ – dynamic viscosity, [uPa·s]
μ_c – $\dot{m}_c/\dot{m}_{in}$, cold mass-flow ratio
μ_{JT} – J-T coefficient, [°CMPa^{-1}]
ν – kinematic viscosity [cm^{2}s^{-1}]
ρ – density [kgm^{-3}]
τ – shear stress, [Pa]
Φ – diameter, [mm]

Subscript

c – cold stream, cold end
cham – vortex tube chamber
h – hot stream, hot end
i – position along the radial direction
in – inlet
t – tangential

References

[1] Hilsch, R., The Use of the Expansion of Gases in a Centrifugal Field as Cooling Process, *Review of Scientific Instruments*, *18* (1947), 2, pp. 108-113
[2] Han, X., *et al.*, The Influence of Working Gas Characteristics on Energy Separation of Vortex Tube, *Applied Thermal Engineering*, *61* (2013), 2, pp. 171-177
[3] Kargaran, M., *et al*., The Second Law Analysis of Natural Gas Behavior within a Vortex Tube, *Thermal Science*, *17* (2013), 4, pp. 1079-1092
[4] Aydin, O., Baki, M., An Experimental Study on the Design Parameters of a Counterflow Vortex Tube, *Energy*, *31* (2006), 14, pp. 2763-2772
[5] Khazaei, H., *et al*., Effects of Gas Properties and Geometrical Parameters on Performance of a Vortex Tube, *Scientia Iranica*, *19* (2012), 3, pp. 454-462
[6] Thakare, H. R., Parekh, A. D., The CFD Analysis of Energy Separation of Vortex Tube Employing Different Gases, Turbulence Models and Discretisation Schemes, *International Journal of Heat and Mass Transfer*, (2014), 78, pp. 360-370
[7] Pourmahmoud, N., *et al.*, Computational Fluid Dynamics Analysis of the Influence of Injection Nozzle Lateral Outflow on the Performance of Ranque-Hilsch Vortex Tube, *Thermal Science*, *18* (2014), 4, pp. 1191-1201
[8] Rahbar, N., *et al*., Numerical Investigation on Flow Behavior and Energy Separation in a Micro-Scale Vortex Tube, *Thermal Science*, *19* (2015), 2, pp. 619-630
[9] Frohlingsdorf, W., Unger, H., Numerical Investigations of the Compressible Flow and the Energy Separation in the Ranque-Hilsch Vortex Tube, *International Journal of Heat and Mass Transfer*, *42* (1999), 3, pp. 415-422
[10] Karimi-Esfahani, M., *et al*., Predicting Optimum Vortex Tube Performance Using a Simplified CFD Model, *Proceedings*, 12th Annual Conference of the CFD Society of Canada, Ottawa, Canada, 2004
[11] Aljuwayhel, N. F., *et al*., Parametric and Internal Study of the Vortex Tube Using a CFD Model, *International Journal of Refrigeration*, *28* (2005), 3, pp. 442-450
[12] Nezhad, A. H., Shamsoddini, R., Numerical 3-D Analysis of the Mechanism of Flow and Heat Transfer in a Vortex Tube, *Thermal Science*, *13* (2009), 4, pp. 183-196
[13] Dutta, T., *et al*., Comparison of Different Turbulence Models in Predicting the Temperature Separation in a Ranque-Hilsch Vortex Tube, *International Journal of Refrigeration*, *33* (2010), 4, pp. 783-792

[14] Nellis, G. F., Klein, S. A., The Application of Vortex Tubes to Refrigeration Cycles, *Proceedings*, International Refrigeration and Air Conditioning Conference, Purdue Univeristy, Purdue, Ind., USA, 2002, p. 537
[15] Sarkar, J., Cycle Parameter Optimization of Vortex Tube Expansion Transcritical CO_2 System, *Proceedings*, *International Journal of Thermal Sciences*, *48* (2009), 9, pp. 1823-1828
[16] Fang, Y., *et al.*, Evaluation on Cycle Performance of R161 as a Drop-in Replacement for R407C in Small-Scale Air Conditioning Systems, *Journal of Thermal Science*, *31* (2022), Aug., pp. 2068-2076
[17] Wang, Z., Suen, K. O., Numerical Comparisons of the Thermal Behaviour of Air and Refrigerants in the Vortex Tube, *Applied Thermal Engineering*, *164* (2020), 114515
[18] Hirsch, C., Numerical Computation of Internal and External Flows, in: *Fundamentals of Numerical Discretization*, John Wiley and Sons, Inc., New York, USA, 1988
[19] ***, ANSYS, I. ANSYS Fluent Theory Guide, Release 15.0. 2013
[20] Wang, Z., Incorporation of a Vortex Tube in Thermal Systems – Refrigerants Screening and System Integrations, Ph. D. thesis, University College London, London, UK, 2018
[21] Eiamsa-ard, S., Experimental Investigation of Energy Separation in a Counter-Flow Ranque-Hilsch Vortex Tube with Multiple Inlet Snail Entries, *International Communications in Heat and Mass Transfer*, *37* (2010), 6, pp. 637-643
[22] Shannak, B. A., Temperature Separation and Friction Losses in Vortex Tube, *Heat and Mass Transfer*, *40* (2004), 10, pp. 779-785
[23] Gao, C., Experimental Study on the Ranque-Hilsch Vortex Tube, Ph. D. thesis, Eindhoven University of Technology, Eindhoven, The Netherlands, 2005
[24] Xue, Y., *et al*., The Expansion Process in a Counter Flow Vortex Tube, *Journal of Vortex Science and Technology*, *1* (2015), 2
[25] Lemmon, E. W., *et al*., The NIST Standard Reference Database 23: Reference Fluid Thermodynamic and Transport Properties-REFPROP, Version 8.0. 2007, National Institute of Standards and Technology, Standard Reference Data Program, Gaithersburg, Md., USA, 2006
[26] Ghoshdastidar, P. S., *Heat Transfer*, 2nd ed., Oxford University Press, Oxford, UK, 2012
[27] Lautrup, B., Physics of Continuous Matter, in: *Exotic and Everyday Phenomena in the Macroscopic World*, 2nd ed., CRC Press, Boca Raton, Fla., USA, 2011
[28] Han, K. H., *et al*., Cooling Domain Prediction of HFC and HCFC Refrigerant with Joule-Thomson Coefficient, *Journal of Industrial and Engineering Chemistry*, *18* (2012), 2, pp. 617-622
[29] Abbas, R., *et al*., Joule-Thomson Coefficients and Joule-Thomson Inversion Curves for Pure Compounds and Binary Systems Predicted with the Group Contribution Equation of State VTPR, *Fluid Phase Equilibria*, *306* (2011), 2, pp. 181-189

Paper submitted: September 26, 2022
Paper revised: November 1, 2022
Paper accepted: November 4, 2022